Experimental Study of Rotor/Body Aerodynamic Interactions

Nai-pei Bi* and J. Gordon Leishman†
University of Maryland, College Park, Maryland

Results are presented that quantify the mutual interactional aerodynamic effects between an articulated rotor and a fuselage consisting of a body of revolution. Wind-tunnel tests were conducted on the isolated body, the isolated rotor, and the rotor/body combination from hover up to an advance ratio of 0.25. Forces and moments on the body and rotor were measured by independent strain-gauge balances. In addition, measurements of both the mean and unsteady pressures on the body were acquired. The results have shown that relatively large forces and pitching moments are created on the body by the presence of the rotor. These loads were significantly affected by variations in both rotor thrust and advance ratio. In turn, the presence of the body produces a moderate increase in rotor thrust and a reduction in power required relative to the isolated rotor performance. Unsteady pressure fluctuations on the body were extremely significant and generally exceeded the mean pressure values. These unsteady pressures were present over the full range of test conditions and appeared to arise from periodic passage of the rotor blades, coupled with either close interactions or direct impingement of discrete wake vortices with the body.

Nomenclature

b = number of blades
C_p = mean static pressure coefficient, $(p - p_\infty)/q_\infty$
C'_p = normalized pressure coefficient, $100(p - p_\infty)/[(1/2)\,\rho\Omega^2R^2]$
C^u_p = normalized unsteady pressure coefficient, $100(p^u - p_\infty)/[(1/2)\rho\Omega^2R^2]$
C_T = rotor thrust coefficient, $T/(\pi\rho\Omega^2R^2)$
C_Q = rotor power coefficient, $Q/(\pi\rho\Omega^2R^5)$
c = blade chord, m
L = body length, m
L_f = body lift in wind axis, N or lbf
M_f = body pitching moment in wind axis, Nm or in.lb
p = time averaged static pressure, Pa
p^u = unsteady component of pressure, Pa
p_∞ = freestream static pressure, Pa
q_∞ = freestream dynamic pressure, $(1/2)\rho V^2_\infty$, Pa
R = rotor radius, m
T = rotor thrust, N
V_∞ = tunnel freestream velocity, m/s
x_f = distance aft of body nose, m
α_s = shaft tilt angle, deg
θ_c = collective pitch angle, deg
μ = advance ratio, $V_\infty/\Omega R$
ρ = air density, kg/m^3
σ = rotor solidity, $bc/\pi R$
Ψ = blade azimuth angle, deg
Ω = rotor rotational frequency, rad/s

I. Introduction

In recent years, increasing attention has been paid to the interactional aerodynamic phenomena encountered on rotorcraft. It is now well known that rotorcraft operate in a highly complex three-dimensional and unsteady flowfield, due primarily to the strong vortical nature of the main rotor wake. The main rotor wake can also affect the flowfield structure near other components of the aircraft, such as the airframe, empennage, or tail rotor. These strongly interdependent phenomena can cause complex and undesirable effects, the consequences of which can affect the performance and handling qualities of the aircraft.

Of course, the severity of the problems actually encountered depends on the relative location of the separate components of the aircraft, as well as their size, shape, and type of wake produced. The various interactional effects encountered will also be a function of the flight conditions in which the aircraft operates. For example, when the aircraft is accelerating, climbing, descending, or maneuvering, the interactional effects encountered may be different in both magnitude and location compared with those encountered under steady level flight conditions. The handling problems encountered on the AH-64 Apache due to unexpectedly high downwash velocities on the horizontal stabilizer[1] provides a classic example of the complex nature of interactional effects under different flight conditions. Since comprehensive analytical tools to model wake/fuselage/tailplane interactional effects were not available, many expensive and time-consuming flight tests were required to meet the handling quality requirements of this aircraft.

Current design requirements for rotorcraft indicate that the next generation of aircraft will have higher blade loadings. Since this results in a rotor wake with greater tip vortex strengths, stronger wake/airframe interactional effects are possible. Other design requirements, such as improved agility and the need to transport rotorcraft on cargo aircraft, have resulted in smaller clearances between the main rotor and the fuselage. As shown by Wilson and Mineck[2] and Sheridan and Smith,[3] reducing the spacing between the rotor and the fuselage can intensify interactional effects considerably. Thus, a capability to understand and confidently predict interactional aerodynamic phenomena is imperative in the successful design of new rotorcraft.

There have been a number of both experimental and theoretical investigations that have addressed these interactional problems. Wind-tunnel experiments by Wilson and Mineck,[2] Sheridan and Smith,[3] Smith and Betzina,[4] and McMahon et al.,[5] among others, have all shown that substantial pressure loads are induced on the fuselage by the main rotor wake. Balch[6] has also shown that the presence of a tail rotor produces further interactional effects. The works of Komerath et al.[7] and Brand et al.[8] have shown that the unsteady pressure fluctuations can be the most prominent form of loading over certain parts of the fuselage.

Received May 8, 1989; presented as Paper 89-2211 at the AIAA 7th Applied Aerodynamics Conference, Seattle, WA, July 31–Aug. 2, 1989; revision received Oct. 6, 1989.

*Graduate Research Assistant, Center for Rotorcraft Education and Research, Department of Aerospace Engineering. Student Member AIAA.

†Assistant Professor, Center for Rotorcraft Education and Research, Department of Aerospace Engineering. Member AIAA.

Besides the influence of the rotor wake(s) on the airframe loads, the airframe also affects the performance of the rotor. Wilby et al.[9] have shown that in forward flight fuselage induced upwash velocities can provide a perturbation to the aerodynamic angle of attack over the front of the rotor disk and can significantly affect the blade loads and hub response. Smith[10] shows that the wake distortion associated with fuselage interactions can generate significant rotor wake interactions that may trigger a torsional aeroelastic response of the blade, leading to premature retreating blade stall. Various other authors, including Johnson and Yamauchi[11] and Fledel et al.[12] have also emphasized the necessity to account for interactional aerodynamic effects in an aeroelastic analysis of the rotor.

Despite the significant advances that have been made in both experimental and theoretical interactional aerodynamics, there are still many features of the interaction mechanisms that are not well understood. Outstanding problems include the physical understanding of wake distortion caused by the fuselage and empennage, the nature of the separated flow behind the rotor hub pylon, the effect of the main rotor wake on horizontal and vertical stabilizers, the effects of the fuselage on the rotor performance and aeroelastic behavior, and the mechanisms of main rotor/tail rotor wake interaction. Because of this, the modeling of interactional phenomena is at a much less developed stage than isolated component analysis.

Most theoretical studies have concentrated on predicting the effects of the rotor wake on the fuselage loads. A good compilation of various methods can be found in a recent paper by Rand.[13] The most recent theoretical works have used surface singularity methods to represent the fuselage coupled with sophisticated prescribed or free-wake analyses for the rotor. The works of Clark and Maskew,[14,15] Berry,[16] Lorber and Egolf,[17] and Quackenbush and Bliss[18] are notable examples. In addition, the works of Gangwani[19] and Mello[20] are also noteworthy since attention is placed on computing the rotor wake effects on lifting surfaces such as horizontal stabilizers. All of these methods have shown promising predictions for both the steady and unsteady induced airloads on the fuselage and empennage. However, only very limited validation with test data has been performed. Further validation is required if these analyses are to be used confidently as future design tools.

To gain a better understanding of these interactional phenomena and to validate and improve upon the various theoretical analyses, it is clear that a significant amount of detailed experimental data is required. Most existing data are for complex geometrical configurations from which it is difficult to isolate the effects of the various flow phenomena of the separate parts of the airframe. This paucity of experimental data hinders the continued development and validation of predictive models. To this end, this paper describes some results from an experiment designed to investigate systematically interactional aerodynamic problems that can exist between a rotor and a geometrically simple body representing a helicopter fuselage. The long-term objectives of this work are to gain an improved physical understanding as to how interactional effects influence the fuselage and empennage loads, as well as the performance of the rotor itself. Initial results from this experiment were reported by Leishman et al.[21] The primary objective in this paper is to extend the discussion of these results and to detail the effects of the rotor wake on the body airloads. Results from the experiment show that the loads on the body in the presence of the rotor wake are very complicated and highly unsteady due to both blade passage and wake induced effects.

II. Description of the Experiment

The configuration tested was a 1.65-m (65-in) diam four-bladed rotor with a fully articulated hub and an idealized, but representative, helicopter fuselage comprising a body of revolution. The general arrangement of the rotor and body is shown in Fig. 1. The rotor consisted of a fully articulated hub, drive shaft, and conventional swashplate arrangement. The hub was unscaled and had a nominal diameter (excluding blade pitch attachments) of 8% relative to the rotor diameter. The rotor hub contained four coincident flap and lead-lag hinges with a hinge offset at 6.53% radius. The pitch assembly of each blade was attached to the hub through a pitch bearing. Collective and cyclic pitch angles were set remotely by positioning the swashplate by means of three electromechanical actuators. The rotor blades were of rectangular planform with a chord of 6.35 cm (2.5 in.). These blades had 12 deg of linear (nose down) twist and used NASA RC410 and RC310 airfoil sections. The blades were structurally very stiff relative to a full-scale rotor in order to minimize aeroelastic effects. Power to the rotor was supplied by a 30 kW (40 hp) hydraulic motor through a belt-driven transmission.

The body geometry selected for this study was designed specifically to be easily modeled analytically. At the same time, some importance was placed on keeping the shape reasonably representative of a helicopter fuselage, i.e., a main body with a long tail boom. The particular body shape selected was a body of revolution. Its shape is defined theoretically as the dividing streamline that exists when superimposing the potential functions of a point three-dimensional source and two three-dimensional sinks in a uniform flow.[22] The 2.5:1-diam taper of the body was designed to be sufficiently moderate to avoid significant flow separations. The body model was constructed from glass-fiber composite shells mounted on to an aluminum frame. The spacing between the rotor and the centerline of the body was 29% of rotor radius,

Table 1 Rotor and fuselage geometry

Number of blades, b	4
Rotor radius, R	0.8255 m (32.5 in.)
Blade chord, c	0.0635 m (2.5 in.)
Rotor solidity, $bc/\pi R$	0.098
Blade twist (linear)	−12 deg
Blade taper ratio	1.0
Rotor airfoils	NASA RC(3), RC(4) series
Fuselage length, L	1.94 m (76.5 in.)
Fuselage max. diameter	0.254 m (10.0 in.)
Fuselage taper ratio	2.5:1

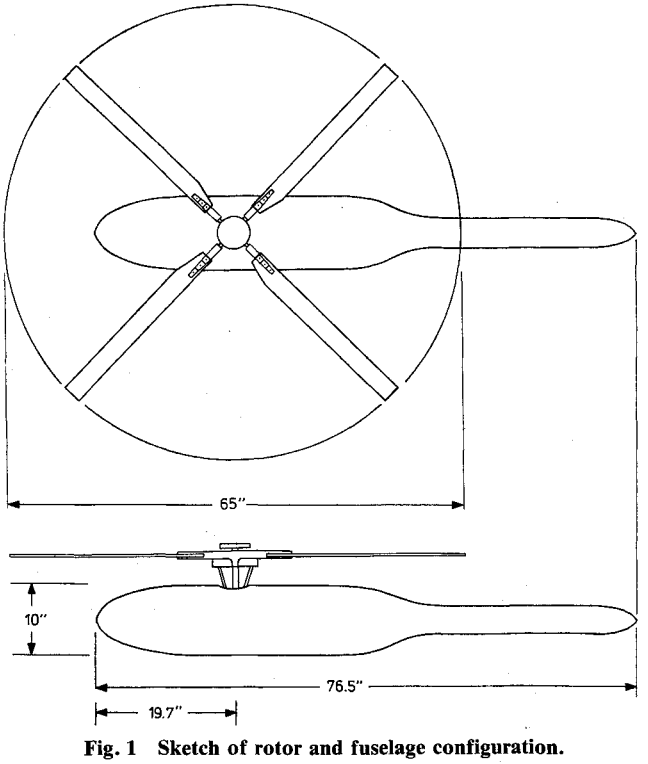

Fig. 1 Sketch of rotor and fuselage configuration.

Table 2 Estimated measurement errors

Parameter	Estimated error
Wind speed, V_∞	±1%
Shaft angle, α_s	±0.05 deg
Collective pitch angle, θ_c	±0.1 deg
Advance ratio	±2%
Rotor forces	±0.5%
Rotor moments	±0.5%
Fuselage forces	±0.5%
Fuselage moment	±0.5%
Steady pressures	±1.5%
Unsteady pressures	±1.5%

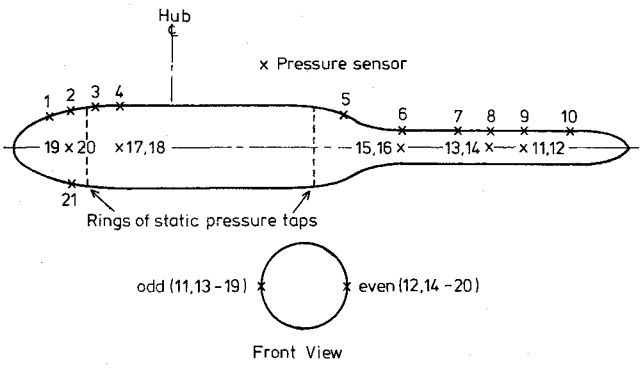

Fig. 2 Locations of pressure measurements.

which is about 14% of the rotor radius above the thickest part of the fuselage. This spacing was held constant during the present series of experiments, although provision has been made to increase the spacing for future experiments. The geometric characteristics of the rotor and body are summarized in Table 1.

The experiments were performed in the Glenn L. Martin wind tunnel at the University of Maryland. This is a closed-return wind tunnel with a 2.36 × 3.35-m (7.75 × 11-ft) working section. The complete rotor and body assembly was mounted on a steel post that was hinged under the wind-tunnel floor. This allowed the whole rotor and body assembly to be tilted remotely, using a hydraulic actuator connected to the post. The shaft tilt was measured using a calibrated angular displacement transducer mounted at the post hinge.

A. Instrumentation

Primary data consisted of independent strain-gauge balance measurements for the rotor and body loads, along with both steady and unsteady pressure loads at a number of points on the body. Rotor loads were measured with a six component strain-gauge balance. Raw balance measurements were reduced to measurements of the rotor thrust, side force, axial force, pitching moment, rolling moment, and yawing moment using an iterative balance subroutine with second-order interaction terms. A torque disk was used to measure the rotor power. The whole rotor balance was isolated from the transmission by means of a flexible diaphragm coupling. A separate three component strain-gauge balance was used to measure the normal force, pitching moment, and axial force on the body. The estimated accuracy of the various balance measurements are given in Table 2.

Mean static pressures were measured at 142 points on the fuselage using lengths of Tygon tubing connected to a bank of four Scanivalve electromechanical pressure switches with 17-kN/m^2 (2.5-psi) range pressure sensors. Pressure taps were located in three rows along the top and sides of the body and at two circumferential rings at the longitudinal locations shown in Fig. 2. Scanivalve measurements were made by ensemble averaging the measured pressure 1024 times over a 2-s time interval (corresponding to 62 rotor revolutions).

Unsteady pressures were measured using 21 temperature compensated piezoresistive pressure transducers. The pressure sensors were concentrated over the nose and tail of the body, also shown in Fig. 2. These sensors were calibrated individually prior to installation inside the body directly below a small pressure tap. Outputs from the transducers were connected to a CAMAC high-speed data acquisition system that was controlled by a HP1000 A400 minicomputer. Each channel was sampled independently and simultaneously by a high-speed 12-bit A/D converter. Estimated errors in the pressure measurements are given in Table 2.

Time histories of all the pressure transducer responses were logged over 10 rotor revolutions at a single channel sampling frequency of 7936 Hz. This gave a sampling resolution of about 1.4 deg of azimuth. Approximately 54 K data samples were recorded for each test condition. Triggering was enabled by a once-per-revolution pulse initiated from an encoder on the rotor flywheel. This trigger signal was also used to measure the rotor speed. Further details of the overall data acquisition system are given in Ref. 21.

B. Testing Procedures

Data were obtained in forward flight for the isolated body, isolated rotor, and the combined rotor/body configuration. Over 200 test conditions were examined. The rotor was tested without the body to provide a baseline performance specification. For these tests, a minimum body aerodynamic fairing was used to cover the rotor-drive mechanism, as shown in Ref. 21. A potential flow analysis of this fairing shape showed that the induced velocity perturbations in the rotor disk plane due to the presence of the fairing were negligible at all the advance ratios tested in this experiment. Nevertheless, the presence of the fairing does create a minor blockage in the rotor wake at low advance ratios and will affect the rotor performance over what would be obtained if a truly isolated rotor test could be performed. In this paper, any reference to the isolated rotor data refers to data taken with the minimum body fairing.

Deadweight tares of the rotor were determined for the range of shaft angles of attack with the blades on and with them removed. Deadweight tares were also determined for the body model. The aerodynamic tares of the hub were determined throughout the range of shaft angles and advance ratios with the hub rotating at normal speed but without the blades attached. Both deadweight and aerodynamic tares have been removed from the balance data presented in this paper.

For the isolated body tests, balance loads and pressure data were obtained for various wind speeds up to 45 m/s (150 ft/s). For the isolated rotor and combined rotor/body tests, data were obtained over the range of advance ratios, shaft tilts, and collective pitch settings given in Table 3. Data were also measured in hover, but only after removing the wind-tunnel floor and ceiling to minimize flow recirculation problems. Nevertheless, because of an uncertainty in conducting hover tests in a relatively confined location, only a limited amount of hover data were actually acquired. Future hover tests are being conducted on a tower external to the wind-tunnel working section.

In forward flight, the wind speed was slowly increased while the rotor was "flown" to the desired test condition by adjusting cyclic and collective pitch inputs. After reaching the desired advance ratio, data were recorded at prescribed values of collective pitch, as given in Table 3. For each test point, the rotor was trimmed for the particular combination of shaft angle and collective pitch setting by adjusting the longitudinal and lateral cyclic to eliminate the once-per-revolution blade flapping response. This ensured that the rotor tip path plane was perpendicular to the shaft axis and, hence, parallel to the longitudinal centerline of the body.

III. Results and Discussion

A. Isolated Body

The static pressure distribution along the top centerline of the isolated body is shown in Fig. 3 for a shaft angle α_s of 0

and −6 deg. From a stagnation point at the nose, the flow accelerates to a peak and then decreases to approximately the freestream value over the region with the uniform cross section. At the body taper, the flow is briefly decelerated and this is followed by a gradual pressure recovery over the tail region. A comparison of a standard source panel model with the test data is also shown in Fig. 3 for $\alpha_s = 0$ deg. Good correlations were obtained. The comparison was quite satisfactory in the tapered region, indicating that this body shape is essentially free of significant flow separations.

Since the rotor had unscaled hub dimensions relative to the body, a brief series of tests were also conducted to assess the significance of the hub on the body loads prior to installing the blades. For these studies, the hub was spun at the normal rotor speed. The body lift and moment were found to be relatively unaffected by the presence of hub; however, some small changes in the pressure distribution were found. Due to the blockage produced by the hub, a region of increased mean pressure was created immediately upstream. Downstream, there was some evidence to suggest the formation of a wake. These results are discussed further in Ref. 21.

B. Rotor/Body Combination

When the rotor and body were tested together, the pressure distribution along the body was modified considerably. The steady pressure distribution along the top and sides of the body in the presence of the hovering rotor is shown in Fig. 4 for $C_T/\sigma \approx 0.08$. These data, and all subsequent steady pressure data, are presented as pressure coefficients nondimensionalized with respect to rotor tip speed. This is a convenient parameter here as it gives a true measure of the actual pressure on the body. It can be seen from Fig. 4 that there are significant increases in pressure over the top of the body in regions affected by the increased dynamic pressure below the rotor. Also shown are significant reductions in pressure on the sides of the body. As a result, the boundary of the rotor wake is clearly quite defined for this hover case. It is interesting that even in hover there is some difference between the pressures on the right and left sides of the body.

The effect of rotor thrust on the body pressure distribution in forward flight at $\mu = 0.05$ is shown in Fig. 5. Only the pressure distributions along the top and the left side of the body are shown here for clarity. With the increased thrust, the total pressure in the rotor wake is higher and, hence, the pressures increase along the top of the body. Since in forward flight the highest downwash velocity is biased toward the rear of the rotor disk, the induced flow velocities produce a suction pressure mainly over the sides of the rear body. An increase in thrust is accompanied by increased downwash velocities, hence, the suction loads on the sides of the body are also increased.

In Fig. 6, the static pressure on the left and right sides of the body is shown at advance ratios of 0.05, 0.10, and 0.20 and at the same nominal thrust of $C_T/\sigma \approx 0.08$. It can be seen that increasing the advance ratio moves the suction peaks further aft along the body. In fact, the maximum suction pressures are significantly attenuated with increasing advance ratio even though the rotor thrust is maintained. The trends shown in Figs. 5 and 6 are, in fact, a direct consequence of changes in strength and position of the rotor wake relative to the body. Since the wake skew angle quickly increases with advance ratio, the wake impinges at points situated further back on the body. It should be remembered that these pressures are normalized but are not scaled with wind speed. Thus, at the nose of the body, where the rotor wake has little effect at these advance ratios, the pressures increase with the square of the tunnel wind speed. It should also be noted that the high adverse pressure gradient downstream of the suction peak indicates that the boundary layer on the body may be more susceptible to separation. Whereas this is unlikely to be a serious problem for this particular body shape, it is another consequence of the wake/body interaction process that must be borne in mind for general body configurations.

It can also be seen from Fig. 6 that at low advance ratios the pressure distributions are significantly different on each side of the body, with a higher suction peak on the left side. The asymmetric nature of this pressure distribution means that the

Table 3 Range of test parameters

Parameter	Test values
Advance ratios, μ	0.0, 0.05, 0.075, 0.1, 0.125, 0.15, 0.20, 0.25
Wind speed, V_∞, m/s	0, 8, 12, 16, 20, 24, 32, 40
Shaft angle, α_s	−8, −6, −4, −2 deg
Collective pitch angle, θ_c	4, 6, 8, 10, 11, 12 deg
Rotor speed	1860 rpm (31 Hz)
Rotor hover tip Mach no.	0.48

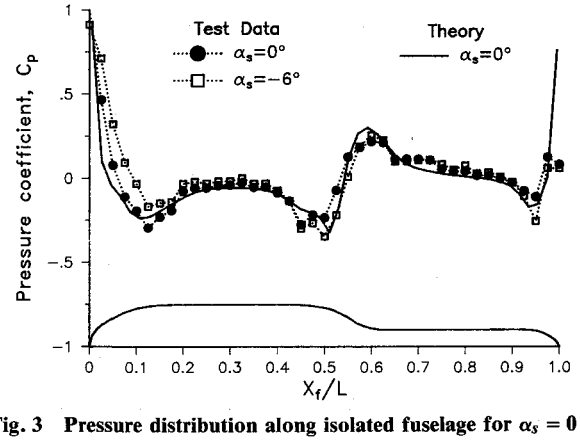

Fig. 3 Pressure distribution along isolated fuselage for $\alpha_s = 0$ deg.

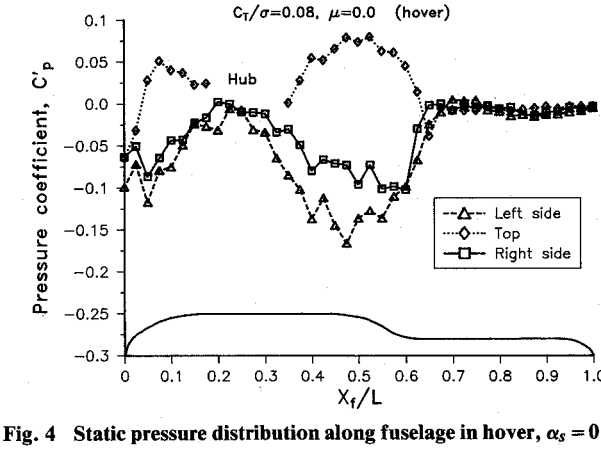

Fig. 4 Static pressure distribution along fuselage in hover, $\alpha_s = 0$ deg.

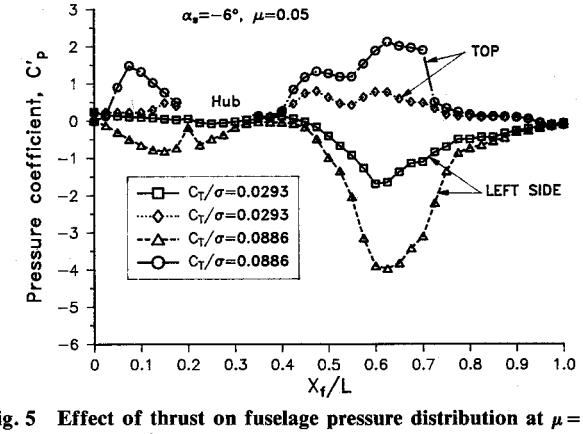

Fig. 5 Effect of thrust on fuselage pressure distribution at $\mu = 0.05$ and 0.15, $\alpha_s = -6$ deg.

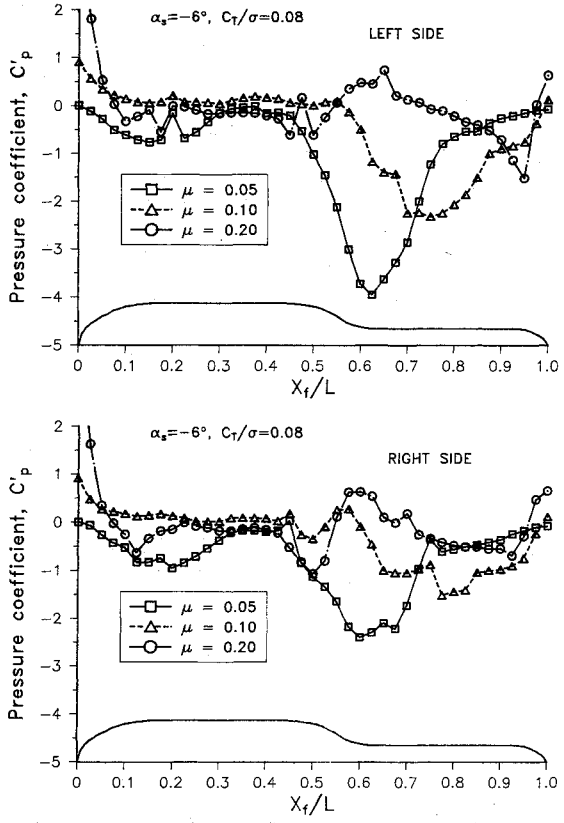

Fig. 6 Effect of advance ratio on fuselage pressure, $C_T/\sigma = 0.07$, $\alpha_s = -6$ deg.

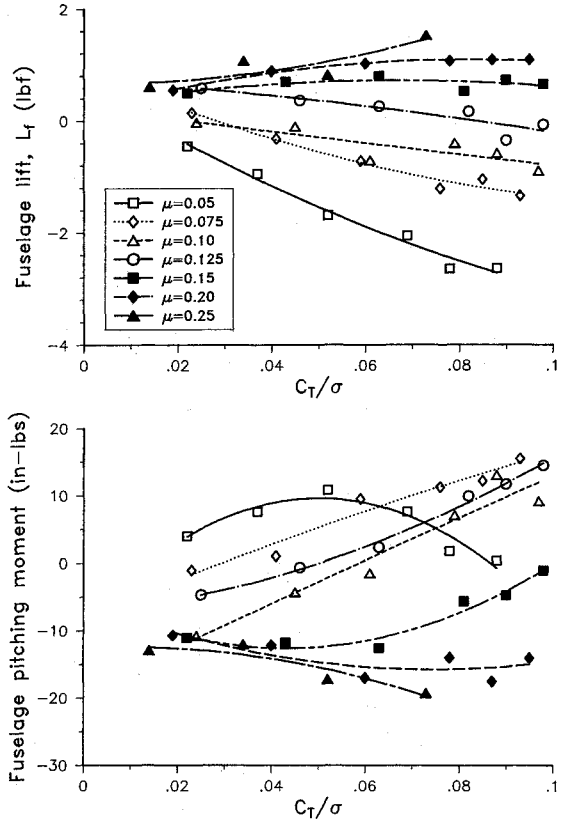

Fig. 7 Effects of rotor thrust on fuselage force and pitching moment, $\alpha_s = -6$ deg.

body will experience a yawing moment. It can be argued that these differences in pressure occur partially because of the asymmetry of the wake induced flow velocities relative to the body centerline. This asymmetry results from the differences in loading distributions across the advancing and retreating sides of the disk as well as from crossflow velocities due to the swirl in the wake. Further tests are planned to measure the velocity field in the vicinity of the body in order to confirm or refute this hypothesis.

C. Fuselage Balance Loads

The effects of the rotor wake on the integrated body loads, as measured by the balance, are shown in Fig. 7 as a function of rotor thrust and for various advance ratios. For advance ratios below about 0.15, the rotor produces a download on the body that increases with increasing rotor thrust, but at the same time quickly diminishes with increasing advance ratio. For advance ratios above 0.15, there is, in fact, a net up-force on the body, confirming the results of Smith and Betzina.[4] At these higher advance ratios, the wake is highly skewed below the rotor. Hence, the wake induced velocities are predominantly streamwise and confined to regions just above the body. The corresponding reduction in local pressure due to the high streamwise velocity results in a positive lift force on the body. It should be noted that the isolated body lift was negligible in comparison to the body lift in the presence of the rotor wake. The drag on the body was also negligible and is not shown here.

The corresponding pitching moment, as shown in Fig. 7, illustrates a somewhat more complicated behavior. Generally, at the lower advance ratios, the pitching moment increases with increasing thrust, indicating that the rotor wake modifies the pressure distribution on the body in such a way as to cause a nose-up pitching moment. In this figure, the pitching moment center is resolved to a point coincident with the hub and body centerlines. This reaffirms the observations from the pressure distributions plotted previously in Fig. 6. As the advance ratio increases, the magnitude of the downwash induced pitching moment reduces and eventually becomes a nose-down moment. It can be seen that there is a sudden change in the pitching moment characteristic at an advance ratio of 0.15. This is because at this advance ratio (and above) the rotor wake is now highly skewed behind the rotor and no longer directly impinges on the body. It is only at the higher thrust coefficients that the wake skew angle is reduced sufficiently to impinge on part of the body. Overall, the changing magnitude of these body pitching moments (as well as the yawing moment) during the transition to forward flight would be important to the helicopter designer from a handling qualities perspective.

D. Rotor Performance

The effect of the body on the rotor thrust and power at $\mu = 0.10$ and 0.25 is shown in Fig. 8, relative to the isolated rotor performance. It was interesting to note that, for a given power, there is an increase in rotor thrust due to the presence of the body. Conversely, at a given thrust setting there is a reduction in power required. These trends were typical over the range of conditions measured in these tests. However, as shown in Fig. 8, as the advance ratio was increased up to 0.25 the body had a significantly less effect on the rotor thrust or power.

There are two mechanisms that may be expected to contribute to this observed behavior. First, at low advance ratio the presence of the body creates a certain amount of blockage in the rotor wake and reduces the magnitude of the induced velocity at points above the centerline of the body. At the blade element level, this corresponds to an increase in leading-edge suction on the airfoil sections (i.e., a reduction in the aft tilt of the local lift vectors) and, therefore, will lead to an increment in blade lift and a reduction in induced drag over parts of the rotor disk. As the advance ratio increases, the rotor wake is swept back by the oncoming flow so the wake blockage effect due to the body becomes significantly less.

Thus, at an advance ratio of about 0.15, the rotor behaves more like it does when operating in isolation.

Second, as the advance ratio increases, the body will also produce its own perturbations to the flowfield, which will in turn modify the local angles of attack in the rotor disk plane (see, for example, Ref. 22). In particular, the rotor should experience an upwash over the front of the body and a downwash over the rear, leading to a redistribution of lift over the disk. However, according to Fig. 8, there is a negligible effect on the mean rotor thrust or power at the highest advance ratio measured with the present body shape. An examination of the control inputs also confirmed that there was no measurable redistribution of the rotor lift up to an advance ratio of 0.25. Nevertheless, it will certainly be expected that the body induced upwash velocities will increasingly affect the rotor loading as the advance ratio becomes even larger or if a less streamlined body shape was to be employed. Future tests are currently planned to address these issues.

E. Unsteady Pressures

Unsteady pressure measurements were made at 21 selected points on the body, as illustrated previously in Fig. 2. Although a large amount of data was recorded, only a selected sample is presented here to illustrate the salient features of the interaction processes. Overall, the unsteady pressure fluctuations on the body were found to be surprisingly large, with transient pressure pulses being measured over the entire body. The dominant frequency of these pressure fluctuations corresponded to 4/rev (4Ω) since four blades were used here. All the unsteady pressure data presented in this paper represent the unsteady fluctuations in pressure C_p^u about the mean value. Again, the unsteady pressures are scaled with respect to rotor tip speed and thus represent a true measure of the interactional pressures. The data are presented as the ensemble average of 10 rotor revolutions. A comparison of the averaged data with data for each individual rotor revolution showed that the pressure responses were periodic and the repeatability was extremely good.

Figure 9 typifies the magnitude of the unsteady pressure loads on the body at an advance ratio of 0.15. Here, the peak-to-peak values of the unsteady pressure at various points along the top of the body are superimposed on the time-averaged (mean) values. It has been shown previously in Fig. 7 that at $\mu = 0.15$ the mean loads on the body are relatively small and are, in fact, close to those measured on the isolated body. Nevertheless, it can be seen clearly from Fig. 9 that at this advance ratio the unsteady pressure fluctuations are still very large in comparison to the mean pressures. This is particularly so over the rear of the body where most of the wake interactions with the body occur. In fact, for nearly every combination of rotor thrust and advance ratio examined, the unsteady fluctuations significantly exceeded the mean pressure values. It was noted, however, that the largest variations in unsteady

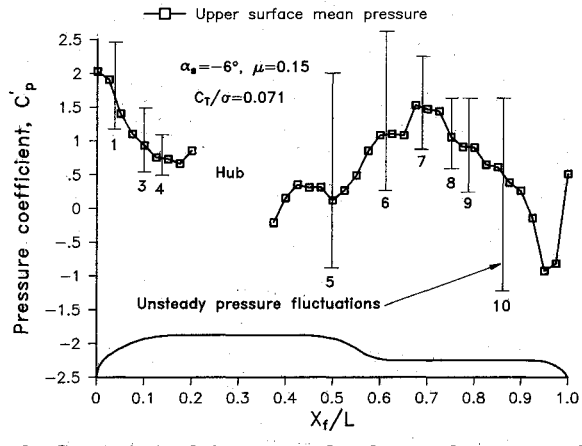

Fig. 9 Comparison of time-averaged and unsteady pressures along the top of fuselage, $\alpha_s = -6$ deg.

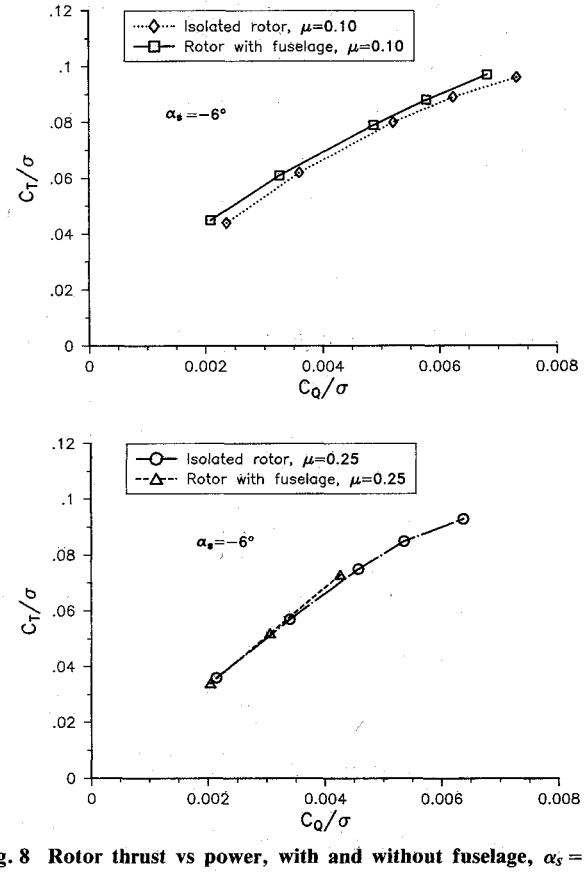

Fig. 8 Rotor thrust vs power, with and without fuselage, $\alpha_s = -6$ deg.

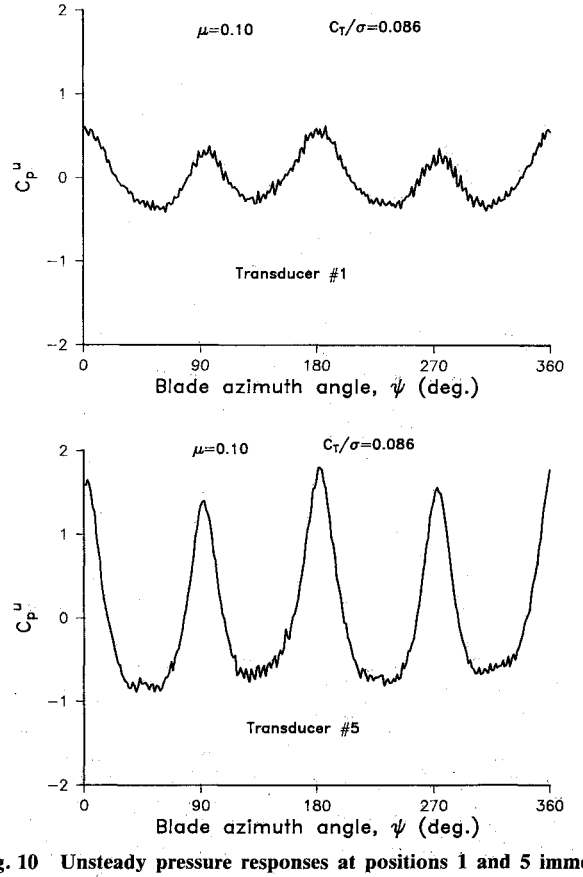

Fig. 10 Unsteady pressure responses at positions 1 and 5 immediately below the rotor, $\alpha_s = -6$ deg.

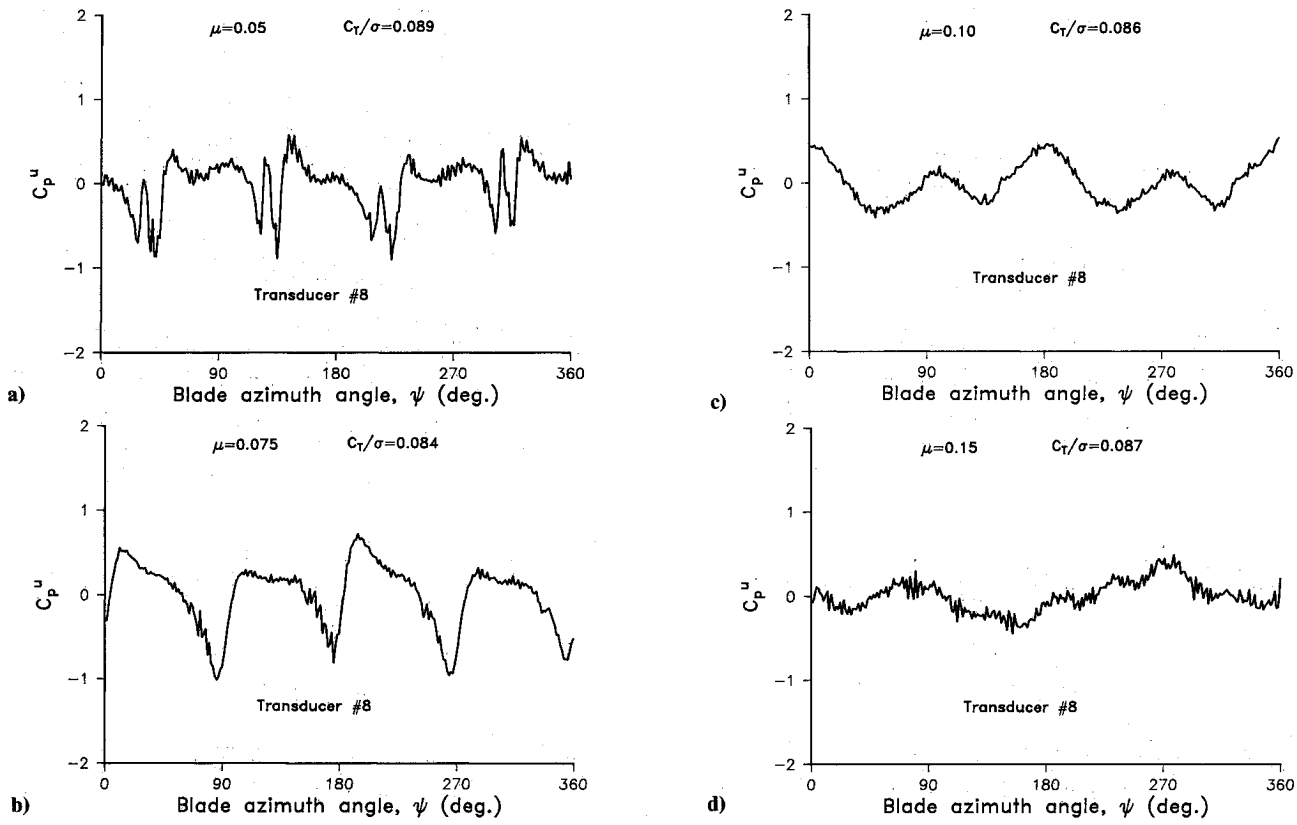

Fig. 11 Unsteady pressure responses on rear fuselage at position 8, $\alpha_s = -6$ deg.

pressures did not necessarily occur in regions with the largest mean pressure. Overall, the results in Fig. 9 reinforce the requirement that any analytical modeling of the aerodynamic interaction process must include unsteady effects; a quasi-steady assumption may not be sufficient to model these measured airloads.

A selection of time histories of the unsteady pressure data, as measured at various points on the body, are shown in Figs. 10–13. In these figures, the time scale is based on blade azimuth angle, which is defined to be zero when a designated (arbitrary) blade passes over the centerline of the rear body. Figure 10 shows the unsteady pressure response below the rotor at locations 1 (on nose) and 5 (aft of hub). It can be seen that both points experience a similar 4Ω pressure pulse although of different magnitudes. Even though these locations are approximately the same distance below the rotor, location 1 is below the root end of the blade (where the lift is low) and location 5 is below the tip (where the lift is much higher). Thus, the pressure pulse at location 5 is obviously much more significant. Pressures at locations 2–4 also responded with a similar 4Ω pulse.

Since, at locations 1–5, the pressure peaks were in-phase with the blade passage, i.e., they occurred at $\psi = 0$, 90, 180, and 270 deg, these particular pressure pulses are clearly induced by the blade pressure loading. From the work of Rand,[13] it appears that these pulse-like pressures due to blade passage can be satisfactorily modeled using an unsteady potential flow analysis of the flowfield. It was also observed that the magnitude and characteristic envelope of the pressure pulses measured at points directly below the rotor were primarily a function of rotor thrust and were unaffected by advance ratio, confirming that these responses were indeed a blade passage effect. In general, it was found that the transducer responses at locations 1–7 all responded at the blade passing frequency of 4Ω, although for locations that were not directly below the rotor (6 and 7) the signal peaks were of much lower magnitude and were slightly out of phase with the blade passage (i.e., out of phase with the response of transducers 1–5).

The next part of this discussion concerns the behavior of the pressures on the rear of the body, in particular at points 8–10. These locations typify the pressure responses obtained during both close interaction and direct impingement of the wake vortices on the body surface. The unsteady pressures are plotted for increasing advance ratio in Figs. 11–13 at $C_T/\sigma \approx 0.085$. As the advance ratio was increased from hover up to 0.05, transducer 8 was the first location to exhibit a noticeable change in the character of the pressure signal. It can be seen from Fig. 11a that fairly large pressure transients were obtained at this location. This appears consistent with the reasoning that the convected wake vortices are very close to, if not directly impinging on, the body near to location 8 for $\mu = 0.05$. Also of interest is the occurrence of two closely spaced pressure pulses. It is not clear why this is the case, but it may be an unsteady effect related to the sudden change in the vortex trajectory or even the formation of some secondary vortex disturbance in the boundary layer. This is currently under more detailed study. The responses at points 9 and 10 downstream (Figs. 12a and 13a) appear to be unaffected by the wake impingement process, indicating that the wake vortices are locally split as they are convected over the body.

It can be seen from Figs. 11–13 that as the advance ratio is increased to 0.075, 0.1, and finally to 0.15, the pressure responses at each location change quite dramatically. From Figs. 12b and 13c, the pressure signatures now look similar to that observed in Fig. 11a. In other words, the location of wake impingement moves quickly along the rear body with increasing advance ratio. The pressure transients shown in Figs. 11b, 12c, and 13d are almost sawtooth in character. The progression of this characteristic sawtooth pressure signal aft along the body with increasing advance ratio suggests that this waveform is the result of a close interaction (but not necessarily impingement) of the rotor wake vortices on the body. It should be noted from Figs. 12c and 13d that while the pressure

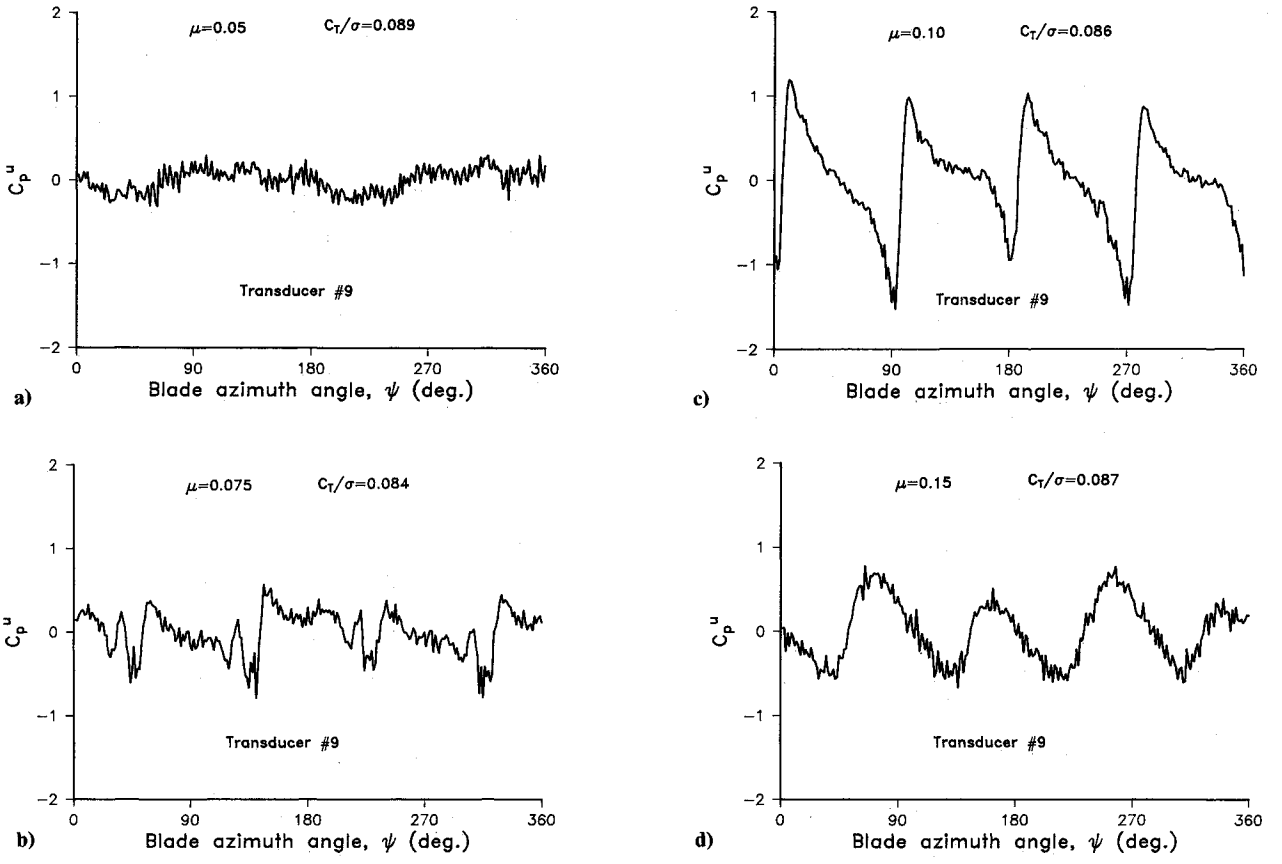

Fig. 12 Unsteady pressure responses on rear fuselage at position 9, $\alpha_s = -6$ deg.

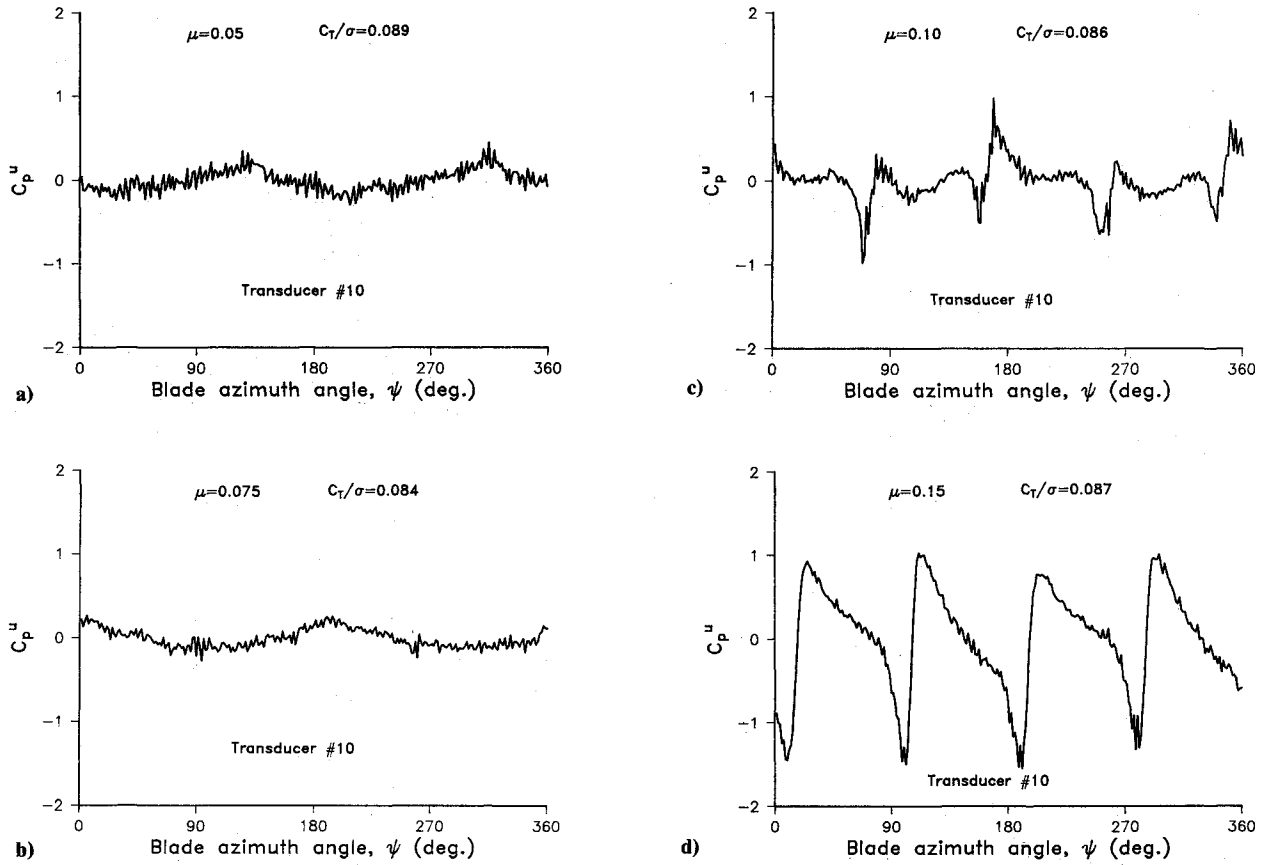

Fig. 13 Unsteady pressure responses on rear fuselage at position 10, $\alpha_s = -6$ deg.

transients are very similar, they are out of phase. This is because increasing the advance ratio affects the spatial position of the convected wake vortices and, hence, the azimuth time at which the wake vortices sweep over the pressure transducer. It can be seen from Fig. 11d that once the rear edge of the rotor wake extends toward the tail end of the body, the pressures at points contained within the rotor wake region (but downstream of the rotor disk) return to their relatively quiescent state.

F. Analytical Study

A parallel analytical investigation was conducted using a surface singularity model with a distorted wake to help identify points on the body that may be in close proximity to the convected rotor wake tip vortices. This in-house developed model is fully unsteady and also contains various coupling strategies to ensure that the wake filaments are further distorted when in close proximity to the body. The model is similar to that developed by Lorber et al.[17] Sample wake geometries (in the form of a wire frame plot) for $C_T/\sigma = 0.075$ and for advance ratios of 0.075, 0.1, and 0.15 are shown in Fig. 14. It can be seen that the tip vortices are convected below and behind the rotor. The locations of wake impingement on the body are reasonably consistent to those inferred from the experimental measurements. However, the predictions of the actual body pressures (not shown here) were only moderately successful and reaffirmed the inherent difficulties of modeling the wake/body interaction process with what is basically a potential flow model. Although more comprehensive and sophisticated computer models for interactional airloads are now becoming available, e.g., Refs. 16 and 17, these models have also experienced difficulties in predicting the unsteady body pressures. The new experimental data presented in this paper, on what is still basically a simple configuration, pose a further challenge for such predictive models.

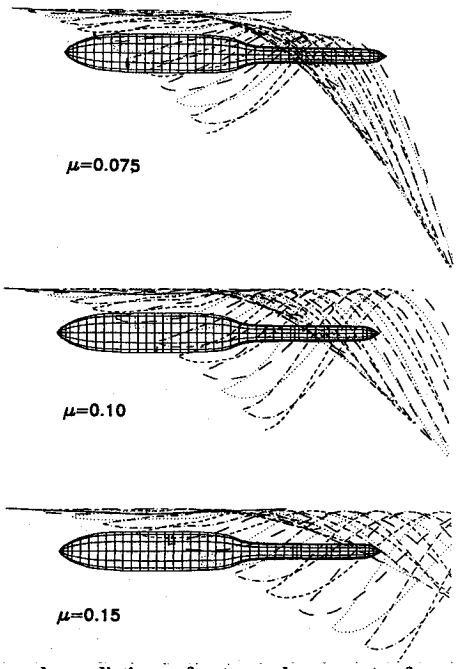

Fig. 14 Sample predictions of rotor wake geometry for various advance ratios.

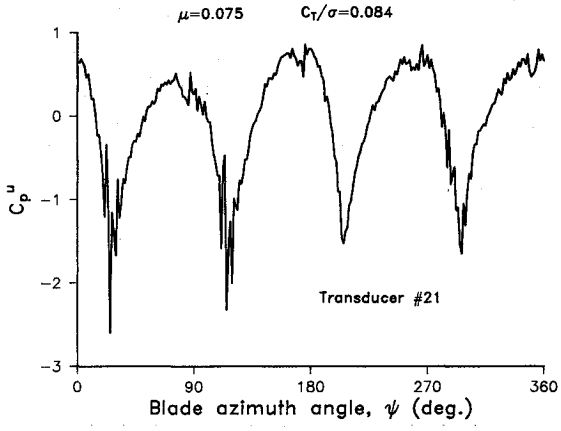

Fig. 15 Unsteady pressure responses below fuselage at position 21, $\alpha_s = -6$ deg.

It can also be seen from the calculations in Fig. 14 that wake vortex interactions with the body may be possible over the nose region at low advance ratio. However, a careful examination of the pressure responses at points 1–4 showed that all measurements were similar to those in Fig. 10, and no combination of thrust or advance ratio produced a pressure signal that could be considered symptomatic of wake impingement on the nose. This was, nevertheless, a slightly surprizing result, as it was initially expected that at least some influence of the wake vortices should be felt over part of the nose region. Further studies using flow visualization techniques have, in fact, confirmed that the rotor wake vortices lie above the tip path plane at the leading edge of the disk and do not come particularly close to the body upstream of the hub. This is true regardless of whether the body is present or not. Furthermore, significant rotor wake distortions have been observed over the rear of the body. Thus, this reaffirms the need to carefully validate predictions of the rotor wake geometry against experimental measurements, with and without the presence of the body.

It was noted, however, that the pressures on the sides (19 and 20) and underside of the body nose (21) did experience responses indicative of close wake vortices. In fact, point 21 on the underside showed an interesting behavior at low advance ratios, as shown in Fig. 15. Here, there is an extremely large induced pressure and is almost certainly due to the close interaction with a rotor tip vortex. It should be noted, however, that the characteristic envelope of the signal is somewhat different to the wake interactions obtained on the upper body surface. Further experiments are planned to examine the detailed nature of the wake structure and the vortex impingement on the body.

IV. Conclusions

A series of wind-tunnel experiments have been conducted to quantify the effects of aerodynamic interactions that can exist between a rotor and a body of revolution. Measurements were made on both the rotor and the body in an attempt to understand more fully the significance of interactional aerodynamic effects on a helicopter rotor/fuselage configuration. The results provide a new and much needed data base of information that can be used to help validate predictive codes.

Results from the study reaffirm that the interaction of a rotor wake with a body is an extremely complex and highly unsteady process. The rotor wake significantly modifies the forces and moments on the body to the extent that they will certainly affect the handling qualities of a full-scale aircraft. Furthermore, the amplitude of the unsteady pressures on the body were found to be extremely large and, under nearly all the conditions examined, significantly exceeded the mean (time-averaged) pressures. This reinforces the requirement that any theoretical analysis of the interactional flowfield must include unsteady effects to account for these loads.

Specific findings from this study suggest that the rotor affects the body loads via four basic mechanisms:

1) A significant redistribution of mean surface pressure in regions of high downwash velocity induced by the rotor. At low advance ratios, this produces a download and nose-up pitching moment on the body. At higher advance ratios, the rotor induced wake velocities are predominantly streamwise

and this results in an up-force and nose-down pitching moment on the body.

2) Strong pressure pulses induced on the body in regions immediately below the rotor. This is an unsteady effect induced by the passage of the lifting blade sections over a fixed point. These loads are sensitive to rotor thrust but are independent of advance ratio.

3) Strong induced pressure loads due to the convection of rotor wake vortices downstream over the top of the body. The magnitude and phasing of these induced pressures are sensitive to both thrust and advance ratio.

4) Induced pressure transients due to direct impingement of the rotor wake vortices on the body. Wake impingement appears to result in a more complex pressure signature, with secondary pressure peaks. It is not clear as to whether these secondary peaks are an unsteady effect due to a sudden change in the wake vortex trajectory or the formation of a secondary disturbance in boundary layer. The location of wake impingement was also sensitive to both rotor thrust and advance ratio.

In addition, there appears to be one primary effect of the body on the rotor performance. A wake blockage effect by the body reduces the magnitude of the induced velocity field below the rotor at low advance ratios. This provides a small increment in rotor thrust and a reduction in power relative to the isolated rotor performance. This effect quickly decreases with increasing advance ratio. It should be noted, however, that at higher advance ratios there may also be a modification to the rotor flowfield due to the induced velocity field produced by the body itself. This was found to have a negligible effect on the rotor performance in the present experiments, although it is likely to become significant for advance ratios above 0.3 or for less streamlined body shapes.

Although the present work has concentrated primarily on measurements of the component loads and body pressures, it is clear that these measurements alone are not sufficient to be able to completely understand the physical mechanisms involved during the rotor wake impingement on the body. Future work will be directed toward both qualitative and quantitative measurements of the detailed flowfield structure during interaction with the body.

Acknowledgments

This research was funded by the U.S. Army Research Office under contract DAAL-03-88-C002. Fritz Oertel Jr. was the technical monitor. The first author was supported by a Fellowship from the Graduate School of the University of Maryland. The authors wish to thank Mike Green and Dhananjay Samak for their expert technical assistance throughout the course of this work. The continued encouragement and support of A. Gessow and I. Chopra is also gratefully acknowledged. A special thanks is due to Jewel Barlow and his technical staff in the Glenn L. Martin wind tunnel for their cooperation and assistance in conducting these experiments.

References

[1]Prouty, R. W., "Development of the Empennage Configuration of the YAH-64 Advanced Attack Helicopter," USAAVRADCOM-TR-82-D-22, Feb. 1983; also Prouty, R., and Amer, K. B., "The YAH-64 Empennage and Tail Rotor—A Technical History," *Proceedings of the 38th Annual Forum of the American Helicopter Society,* AHS, Alexandria, VA, May 1982.

[2]Wilson, J. C., and Mineck, R. E., "Wind-Tunnel Investigation of Helicopter Rotor Wake Effects on Three Helicopter Fuselage Models," NASA TM X-3185, 1975.

[3]Sheridan, P. F., and Smith, R. P., "Interactional Aerodynamics—A New Challenge to Helicopter Technology," American Helicopter Society, Alexandria, VA, Paper 79-59, May 1979.

[4]Smith, C. A., and Betzina, M. D., "Aerodynamic Loads Induced by a Rotor on a Body of Revolution," *Journal of the American Helicopter Society,* Vol. 31, No. 1, 1986, pp. 29–36.

[5]McMahon, H. M., Komerath, N. M., and Hubbard, J. E., "Studies of Rotor-Airframe Interactions in Forward Flight," AIAA Paper 85-5015, Oct. 1985.

[6]Balch, D. T., "Experimental Study of Main Rotor/Tail Rotor/Airframe Interaction in Hover," *Journal of the American Helicopter Society,* Vol. 30, No. 2, 1985, pp. 49–56.

[7]Komerath, N. M., McMahon, H. M., and Hubbard, J. E., "Aerodynamic Interactions between a Rotor and Airframe in Forward Flight," AIAA Paper 85-1606, July 1985.

[8]Brand, A. G., McMahon, H. M., and Komerath, N. M., "Wind Tunnel Data for a Rotorcraft Airframe Interaction Study," School of Aerospace Engineering, Georgia Inst. of Technology, Atlanta, GA, Rept. DAAG29-82-K-0094, July 1986.

[9]Wilby, P. G., Young, C., and Grant, J., "An Investigation of the Influence of Fuselage Flow Field on Rotor Loads and the Effects of Vehicle Configuration," *Vertica,* Vol. 3, No. 2, 1979, pp. 79–94.

[10]Smith, R. V., "Some Effects of Wake Distortion Due to a Fuselage Flow Field on Rotor Thrust Limits," ARO Workshop on Rotor Wake Technology, Raleigh, NC, April 1979.

[11]Johnson, W., and Yamauchi, G. K., "Applications of an Analysis of Axisymmetric Body Effects on Rotor Performance and Loads," Paper No. 3, 10th European Rotorcraft Forum, The Hague, the Netherlands, Aug. 1984.

[12]Fledel, S., Rand, O., and Chopra, I., "Coupled Rotor/Airframe Vibration Analysis," Paper No. 52, 15th European Rotorcraft Forum, Amsterdam, the Netherlands, Sept. 1989.

[13]Rand, O., "The Influence of Interactional Aerodynamics in Rotor/Fuselage Coupled Response," *Proceedings of the Second International Conference on Rotorcraft Basic Research,* College Park, MD, Feb. 1988.

[14]Clark, D. R., and Maskew, B., "Study for Prediction of Rotor/Wake/Fuselage Interference," NASA CR-177340, March 1985.

[15]Clark, D. R., and Maskew, B., "Calculation of Unstudy Rotor Blade Loads and Blade/Fuselage Interference," *Proceedings of the Second International Conference on Rotorcraft Basic Research,* College Park, MD, Feb. 1988.

[16]Berry, J. D., "Prediction of Time-Dependent Fuselage Pressures in the Wake of a Helicopter Rotor," *Proceedings of the Second International Conference on Rotorcraft Basic Research,* College Park, MD, Feb. 1988.

[17]Lorber, P. F., and Egolf, T. A., "An Unsteady Helicopter Rotor-Fuselage Interaction Analysis," NASA CR-4178, Aug. 1988.

[18]Quackenbush, T. R., and Bliss, D. B., "Free Wake Calculation of Rotor Flow Fields for Interactional Aerodynamics," *Proceedings of the 44th Annual Forum of the American Helicopter Society,* AHS, Alexandria, VA, June 1988.

[19]Gangwani, S. T., "Calculation of Rotor Wake Induced Empennage Airloads," *Journal of the American Helicopter Society,* Vol. 28, No. 2, 1983, pp. 37–46.

[20]Mello, O., "Unsteady Loads on Helicopter Lifting Surfaces," M.S. Thesis, Dept. of Aerospace Engineering, Univ. of Maryland, College Park, MD, Dec. 1988.

[21]Leishman, J. G., Bi, N., Samak, D. K., and Green, M., "Investigation of Aerodynamic Interactions Between a Rotor and a Fuselage in Forward Flight," *Proceedings of the 45th Annual Forum of the American Helicopter Society,* AHS, Alexandria, VA, May 1989.

[22]Rand, O., and Gessow, A., "Model for Investigation of Fuselage Influence on Rotor Flowfields," *Journal of Aircraft,* Vol. 26, No. 5, 1989, pp. 401–402.